

Three-dimensional graphene framework with ultra-high sulfur content for a robust lithium–sulfur battery

Benjamin Papandrea^{1,§}, Xu Xu^{1,2,§}, Yuxi Xu¹, Chih-Yen Chen³, Zhaoyang Lin¹, Gongming Wang¹, Yanzhu Luo², Matthew Liu³, Yu Huang^{3,4}, Liqiang Mai² (✉), and Xiangfeng Duan^{1,4} (✉)

¹ Department of Chemistry and Biochemistry, University of California, Los Angeles, CA 90095, USA

² State Key Laboratory of Advanced Technology for Materials Synthesis and Processing, Wuhan University of Technology, Wuhan 430070, China

³ Department of Materials Science and Engineering, University of California, Los Angeles, CA 90095, USA

⁴ California NanoSystems Institute, University of California, Los Angeles, CA 90095, USA

[§] These authors contributed equally to this work.

Received: 18 December 2015

Accepted: 5 January 2016

© Tsinghua University Press and Springer-Verlag Berlin Heidelberg 2016

KEYWORDS

energy storage, graphene framework, three-dimensional (3D)-network, high loading, lithium sulfur battery

ABSTRACT

Lithium–sulfur batteries can deliver significantly higher specific capacity than standard lithium ion batteries, and represent the next generation of energy storage devices for both electric vehicles and mobile devices. However, the lithium–sulfur technology today is plagued with numerous challenges, including poor sulfur conductivity, large volumetric expansion, severe polysulfide shuttling and low sulfur utilization, which prevent its wide-spread adoption in the energy storage industry. Here we report a freestanding three-dimensional (3D) graphene framework for highly efficient loading of sulfur particles and creating a high capacity sulfur cathode. Using a one-pot synthesis method, we show a mechanically robust graphene–sulfur composite can be prepared with the highest sulfur weight content (90% sulfur) reported to date, and can be directly used as the sulfur cathode without additional binders or conductive additives. The graphene–sulfur composite features a highly interconnected graphene network ensuring excellent conductivity and a 3D porous structure allowing efficient ion transport and accommodating large volume expansion. Additionally, the 3D graphene framework can also function as an effective encapsulation layer to retard the polysulfide shuttling effect, thus enabling a highly robust sulfur cathode. Electrochemical studies show that such composite can deliver a highest capacity of 969 mAh·g⁻¹, a record high number achieved for all sulfur cathodes reported to date when normalized by the total mass of the entire electrode. Our studies demonstrate that the 3D graphene framework represents an attractive scaffold material for a high performance lithium sulfur battery cathode, and could enable exciting opportunities for ultra-high capacity energy storage applications.

Address correspondence to Xiangfeng Duan, xduan@chem.ucla.edu; Liqiang Mai, mlq518@whut.edu.cn

1 Introduction

Energy storage devices are of increasing importance for applications in mobile electronics, hybrid electric vehicles, and can also play a critical role in renewable energy harvesting, conversion and storage. The lithium ion battery represents the dominant energy storage technology for mobile power supply today. However, the total capacity of lithium ion batteries is largely limited by the theoretical capacities of the cathode materials such as LiCoO_2 ($272 \text{ mAh}\cdot\text{g}^{-1}$), and LiFePO_4 ($170 \text{ mAh}\cdot\text{g}^{-1}$), and cannot satisfy the increasing consumer demand [1–4]. Lithium sulfur (Li–S) batteries represent the next generation of battery technology, with the sulfur cathode offering a far higher theoretical capacity of $1,675 \text{ mAh}\cdot\text{g}^{-1}$ [5–8]. However, there are many challenges associated with Li–S battery technology today, including the intrinsic insulating properties of sulfur and Li_2S , cathode degradation caused by volume expansion/contraction during discharge/recharge process, and the polysulfide shuttling effect [9–15].

To combat the intrinsic insulating properties of the sulfur, a sulfur cathode is typically prepared by introducing considerable amount of conductive additive and binder to create a composite electrode. Because the conductive additive and binder are typically electrochemically inactive and do not contribute to the energy storage capacity, it is particularly important to minimize the amount of these inactive components and thus maximize the loading ratio of the electrochemically active sulfur in the composite electrodes. Creating a composite electrode with high sulfur content is essential for ensuring high capacity and low production cost for real-world applications [16–22]. However, because of the intrinsically insulating nature and dynamic size change in sulfur, there is considerable challenge in increasing the sulfur-loading ratio while retaining the electrical conductivity and structural integrity of the composite electrode. The majority of literature to date uses a composite electrode with the sulfur amount typically <60% of the total weight of the entire cathode (including sulfur, conductive additive and binder) [23]. Higher sulfur content up to 80% of the total electrode weight has been reported recently, but the performance of such cathode is yet to be optimized [19].

Here we aim to explore a three-dimensional graphene framework (3DGF) as a unique conductive scaffold for efficiently loading sulfur particles to create a high performance sulfur cathode [24–26]. The unique structural characteristics and electrical properties of the 3DGF can effectively address many challenges associated with Li–S battery cathodes. First, the highly porous framework structure can allow efficient incorporation of the active sulfur to ensure a high sulfur content up to 80%–90%. Second, the conjugated graphene sheets form a continuous network to provide efficient electron transport pathway. The conductivity of the 3DGF can reach up to $\sim 1,400 \text{ S}\cdot\text{m}^{-1}$, enough to counter the insulating properties of sulfur and the discharge products. Third, the hierarchical porous network structure can offer a network of open channels for efficient ion transport. Finally, the individual graphene sheets are conjugated and interlocked together to form a monolithic three-dimensional (3D) network that is mechanically strong and can be used as a standalone electrode without extra binders and can withstand repeated expansion and contraction in the charge/discharge cycles [27–32]. Indeed, freestanding 3DGF has recently been explored for Li–S battery electrodes [19, 33, 34]. The 3D graphene–sulfur (3DG–S) cathodes reported to date were typically prepared via a two-step process by first creating 3DGF followed by infiltrating sulfur, typically with a sulfur content of 60%–80% and a highest capacity of only ~ 500 – $625 \text{ mAh}\cdot\text{g}^{-1}$ when normalized by the total weight of the cathode material. Here we report a facile one-pot synthesis method to encapsulate sulfur within a freestanding 3DGF to form a 3DG–S composite electrode with a record-high sulfur content of 90%. When used directly as the Li–S battery cathode without any additives, the 3DG–S composite electrode displays a capacity of $969 \text{ mAh}\cdot\text{g}^{-1}$ (at 0.1 C), the highest ever value achieved for all sulfur cathodes reported to date when normalized by total electrode mass.

2 Results and discussion

Figure 1 schematically highlights the structure of our 3DG–S composite. By uniformly loading sulfur particles into the 3D graphene network, the poor electrical conductivity of sulfur is mitigated by the high electrical

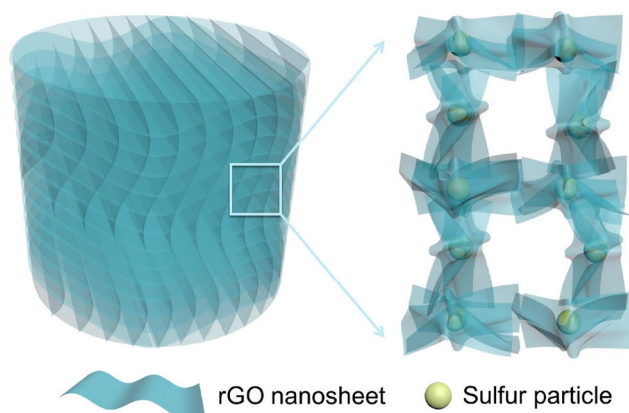


Figure 1 Schematic of freestanding 3D graphene-sulfur composite. The left schematic shows a depiction of the three dimensional structure, and the right schematic illustrates the magnified view of the cross section. The sulfur particles are encapsulated within the 3D graphene pockets.

conductivity of the graphene network. At the same time, the mechanical stress induced by the volume expansion/contraction during the discharge/charge cycles is also well contained by the flexibility and porosity of the graphene framework. Furthermore, the encapsulation of sulfur particles by the 3D graphene pockets can also inhibit the polysulfide shuttling process to ensure the long duration stability of the electrodes [20].

The 3DG-S composite electrode was prepared using a facile one-pot synthesis by mixing $\text{Na}_2\text{S}_2\text{O}_3$ and HCl in the presence of graphene oxide (GO) flakes, where the following reaction took place (Eq. (1)) [35]



The formation of 3DG-S composite is induced by introducing the ascorbic acid to drive the reduction of GO and conjugation of the reduced GO into the 3D

graphene hydrogel with encapsulated sulfur particles. A photograph of the GO solution shows the typical brownish color (Fig. 2(a), left), while the solution of GO with $\text{Na}_2\text{S}_2\text{O}_3$ and HCl (Fig. 2(a), middle) shows milky cloudy suspension indicating the presence of a large number of sulfur particles. Importantly, with the introduction of the ascorbic acid, a mechanically strong freestanding 3DG-S composite hydrogel can be readily obtained. The photograph of the resulting 3DG-S composite hydrogel in the reaction solution (Fig. 2(a), right) shows a freestanding structure and clear supernatant solution indicating that most of the GO and sulfur particles are conjugated together to form the composite hydrogel with essentially negligible GO or sulfur left in solution. The 3DG-S composite hydrogel was then freeze-dried for subsequent studies. In this way, 3DG-S composites with 70%, 80%, 90% and 95% sulfur content (denoted as 3DG-S70, 80, 90 and 95, respectively) can be readily prepared.

We have used X-ray diffraction (XRD) to characterize the 3DG-S90 sample both before and after the reduction process and formation of 3DG-S composite (Fig. 2(b)). The initial broad GO peak at 11.6° diminishes after the reduction with ascorbic acid, and the reduced GO (rGO) peaks appears at around 22.2° , signifying that the reduction of GO was successful. The XRD spectra shows well-defined diffraction peaks for orthorhombic phase sulfur (JCPDS Card No. 08-0247) in both the samples before and after reduction, confirming the successful incorporation of sulfur into the 3D graphene frameworks. It is important to control the exact sulfur content in the 3DG-S composite to ensure optimum cathode performance. To this end, the amount of sulfur particles wrapped within the 3D graphene framework can be readily tuned by controlling the

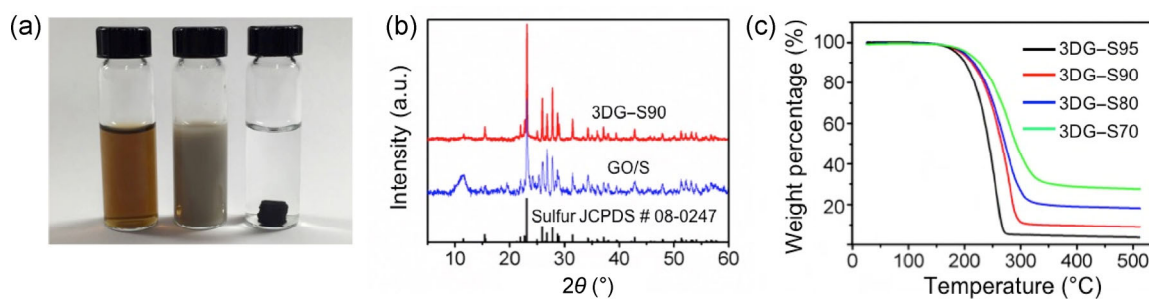


Figure 2 (a) Photograph of the solutions of GO, GO with $\text{Na}_2\text{S}_2\text{O}_3$ and HCl, and after reduction of the GO with ascorbic acid, respectively. (b) Comparison of the XRD of pure S_8 , GO/S and 3DG-S90. (c) TGA of different 3DG-S samples.

concentration of the sulfur precursor in the GO solution. Thermogravimetric analysis (TGA) was performed to determine the amount of sulfur loaded in the composite structure [36, 37]. The TGA studies of the 3DG–S composites show an obvious weight loss when the temperature is increased above 200 °C (Fig. 2(c)), corresponding to sulfur sublimation temperature. To precisely determine the sulfur content, we have also conducted TGA of the pure 3DGF to account for the weight loss contribution from the graphene framework itself (Fig. S1 in the Electronic Supplementary Material (ESM)). After the calibration of weight loss from the pure 3DGF, we can determine the samples with sulfur contents of 70%, 80%, 90%, and 95%. We have also determined the surface area of our 3DG with and without sulfur using methylene blue absorption test as used in previous studies [27, 29], and found that both the 3DG with or without sulfur loading exhibit a highly comparable surface area of approximately 900 m²·g⁻¹ when normalized by the amount of carbon, indicating that the inclusion of the sulfur particles does not significantly impact on the overall structure of the 3D graphene framework.

The scanning electron microscopic (SEM) images of the cross-section view of 3DG–S70, 80, 90, and 95 composite show the highly porous graphene framework structures. The 3DG–S70, 80, 90 show similar porous structures with pore sizes typically on the micron scale and comparable sulfur particle size around 1 μm (Figs. 3(a)–3(c)). When the sulfur content is increased to 95%, the 3DG–S95 shows rather distinct structural features (Fig. 3(d)), with the sulfur particles covering the majority of the graphene sheets and the sample being mechanically very fragile. It should be noted that, for the same amount of graphene, the sulfur mass more than doubles when the sulfur content increases from 90% to 95%.

We have used transmission electron microscopy (TEM) studies to evaluate the encapsulation of sulfur within 3D graphene pockets (Fig. 4(a)). Sulfur particles can be seen wrapped around by the graphene. With the strong electron beam irradiation under the TEM, we melted the enwrapped sulfur particles and observed its dynamic flow within the 3D graphene pocket without leaking out onto the copper grid (Figs. 4(b)–4(f), and Video S1 in the ESM), confirming that

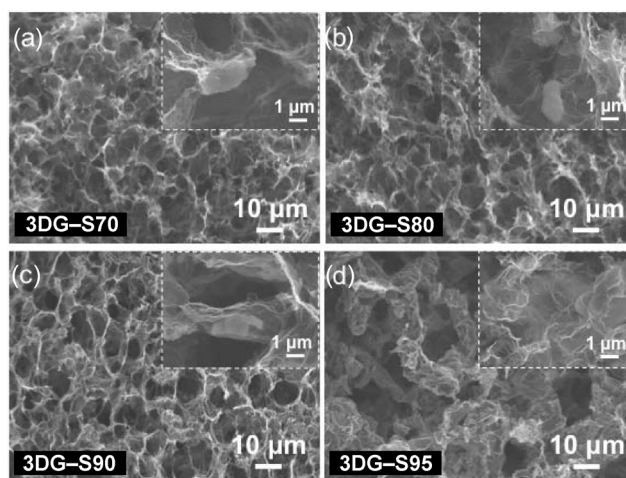


Figure 3 Low- and high-magnification (inset) SEM images of (a) 3DG–S70, (b) 80, (c) 90 and (d) 95, respectively.

the sulfur is well encapsulated within the graphene framework with multi-level pockets. Figures 4(b)–4(d) showcases the melted sulfur flowing across graphene wall-1, but then been stopped by graphene wall-2 of the graphene pocket as seen in Figs. 4(e) and 4(f). This multiwall feature of the 3D graphene pocket can efficiently inhibit the leakage of the liquid sulfur. The solid–liquid phase transformation of sulfur into soluble polysulfide in the electrolyte during the discharge process is similar to the observed melting process, suggesting that encapsulation of sulfur by 3D graphene pockets may be an effective way to retard the polysulfide shuttling effect [38].

With the successful preparation of the mechanically strong 3DG–S composites with ultra-high sulfur content, we have further evaluated their electrochemical performance by directly using the freeze-dried 3DG–S composites as the freestanding cathodes without any other additives. Galvanostatic testing was performed in the voltage range of 1.6–2.6 V (vs. Li⁺/Li). Figure 5(a) shows the discharge/charge curves of 3DG–S90 at 0.1 C. Two plateaus are present, one at 2.32 V and another at 2.08 V, indicative of the formation of long-chain (Li₂S_x, 4 ≤ x ≤ 8) and short-chain polysulfides (Li₂S₂ or Li₂S) [39]. The discharge/charge curves of the 20th and 50th cycles also clearly showcase the two plateaus, indicating the good electrochemical stability of such cathode. On the first cycle, we achieved an extraordinary capacity of 1,070 mAh·g⁻¹ with 90 wt.% sulfur. Figure 5(b) showcases the different 3DG–S

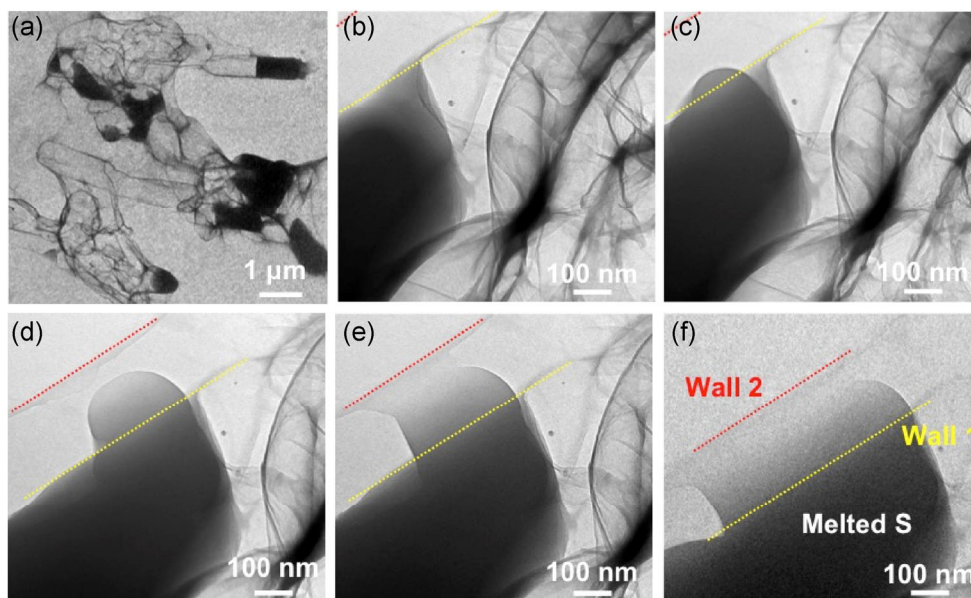


Figure 4 (a) Low-magnification TEM image of sulfur particles encapsulated in the 3D graphene pockets. (b)–(f) Multiple frames of the movement of melted sulfur contained within the graphene pocket. The dotted lines indicate the walls of the graphene pocket.

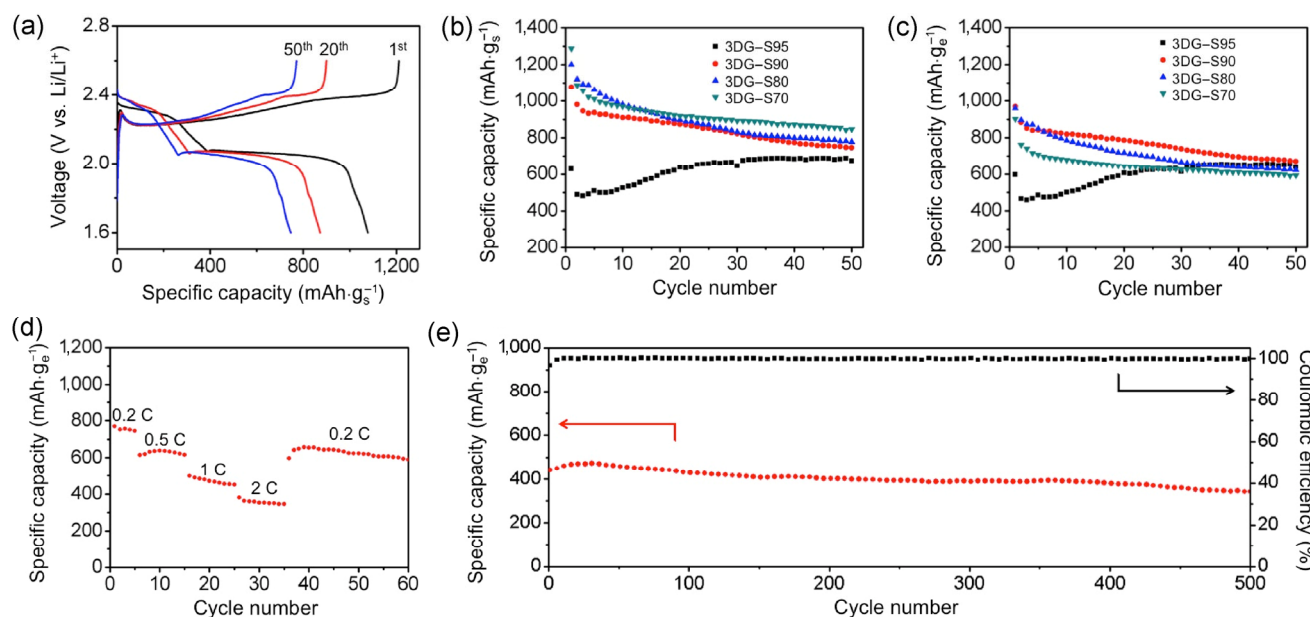


Figure 5 (a) Discharge and recharge profile of the 1st, 20th and 50th cycle of 3DG–S90. (b) and (c) Cycling performance of 3DG–S70, 80, 90, and 95 at 0.1 C with the capacities normalized by (b) only sulfur mass and (c) entire electrode. (d) Rate performance of 3DG–S90 at 0.2 C, 0.5 C, 1 C, and 2 C with the capacities normalized by entire electrode. (e) 3DG–S90 cycling at 1 C for 500 cycles with the capacities normalized by entire electrode.

samples cycling at 0.1 C where the capacity is normalized only by the sulfur content. The initial capacities for 3DG–S70, 80, 90 and 95 are 1,286, 1,200, 1,077 and 628 mAh·g⁻¹, respectively. As expected, when the sulfur loading is lower, the capacity normalized by sulfur tends to be higher, because less sulfur in the

graphene framework means relatively more electron and ion transport pathways to make full usage of the sulfur. After 50 cycles, the capacities decrease to 846, 777, and 746 mAh·g⁻¹ for 3DG–S70, 80 and 90, respectively. It is interesting to note that the specific capacity of 3DG–S95 increases gradually to 673 mAh·g⁻¹

after 50 cycles, which may be attributed to the excessive insulating sulfur in the framework that needs a long activation process to gradually utilize the deep-buried sulfur [19].

A major issue with Li–S battery research is how to normalize electrochemical performance. In lithium ion battery research, there is a standard of about 70 wt.%–80 wt.% active material, and 20 wt.%–30 wt.% binder and conductive additive. For Li–S battery research, researchers usually normalize the capacity by only sulfur. However, with a large variation of sulfur content (30%–60% for most reports) with different electrode preparation [18, 23], it is difficult to properly compare data obtained in different studies. In general, when normalized only by sulfur, the less sulfur, the higher the capacity is expected (see Fig. 5(b)). On the other hand, if we normalize the capacity by the mass of the entire electrode, the 3DG–S90 cathode shows the best performance among all four different samples (Fig. 5(c)). Importantly, when normalized by the entire electrode, 3DG–S90 delivers a specific capacity of 969 mAh·g⁻¹ (at 0.1 C), the highest capacity ever achieved for all sulfur cathodes reported to date (Table 1) [7, 18, 19, 22, 37, 40]. Furthermore, when comparing our capacity at different cycles to literature, our capacity is still the highest (Table S1 in the ESM). Considering the many methods of preparing a Li–S

cathode with high different sulfur content, it is important and essential to display Li–S battery data normalized by entire cathode weight. It is also important to note the C rate is typically normalized by sulfur only. Therefore, if we normalize the power density by total mass of the electrode, the power density of our 3DG–S90 with higher sulfur content would be higher than those of previous reports at the same C rate.

The composite 3DG–S90 is found to have the highest capacity normalized by the entire electrode mass, so it is chosen to investigate the high-rate and cycling performance. Figure 5(d) shows the rate performance of 3DG–S90 normalized by the entire electrode mass from 0.2 to 2 C. The initial capacities at 0.2, 0.5, 1 and 2 C are 772, 615, 500 and 381 mAh·g⁻¹, respectively. It is important to note that due to large intrinsic capacity, the sulfur cathode with 1 C rate can deliver a power density more than one order of magnitude higher than of conventional lithium-ion battery at 1 C rate. The 3DG–S90 cathode exhibits a good cycling response at various current rates and the capacity is able to recover to 657 mAh·g⁻¹ at 0.2 C. Figure 5(e) displays the long-life performance of 3DG–S90 cathode at 1 C. The initial specific discharge capacity is 441 mAh·g⁻¹ normalized by the entire electrode mass. The capacity increases gradually to 473 mAh·g⁻¹ after

Table 1 Comparison of the results of this work to reported results. The sulfur content in the composite refers to the percentage of sulfur used before the addition of conductive additive/binder, whereas the sulfur content in the cathode includes the entire electrode mass. Although our capacity is lower compared to literature when normalized only by sulfur, it is considerably higher when normalized by the entire electrode mass

Ref.	Cathode materials	Sulfur content in the composite (%)	Sulfur content in the cathode (%)	Highest capacity normalized by sulfur mass (mAh·g ⁻¹ at 0.1C)	Highest capacity normalized by electrode mass (mAh·g ⁻¹ at 0.1C)
[19]	Sulfur-graphene sponge	80	80	625	500
[18]	Aligned carbon nanotube/sulfur composite	90	77	737	564
[40]	Pomegranate-like carbon cluster-encapsulated sulfur	70	63	1,200	756
[22]	Sulfur/porous graphitic carbon composites	89	62	864	535
[8]	Nanostructured sulfur/mesoporous carbon materials	70	59	1,320	779
[37]	Monodispersed sulfur nanoparticles on rGO	70	49	1,672	819
This work	3DG–S90	90	90	1,077	969

30 cycles due to the activation process. After 500 cycles, the capacity is $341 \text{ mAh}\cdot\text{g}^{-1}$, corresponding to the capacity retention of 77% and the capacity fading of 0.052% per cycle. After the initial activation process (the first 10 cycles), the Coulombic efficiency stays consistent at 99.5% throughout cycling.

3 Conclusion

We have designed and synthesized a freestanding 3D graphene-sulfur composite using a one-pot synthesis method. The combination of the highly conductive interconnected and mechanically strong 3D graphene and the enwrapped sulfur particles has enabled a high performance sulfur-cathode with a record-high capacity of $969 \text{ mAh}\cdot\text{g}^{-1}$ when normalized by the weight of entire cathode at 0.1 C, and stable cycling endurance up to 500 times at 1 C with a capacity fading of 0.052% per cycle. These results demonstrated that the free-standing 3DGF with ultra-high sulfur content can offer a promising pathway to a highly robust Li-S battery.

4 Experimental

4.1 Graphene oxide synthesis

Graphene oxide suspension was synthesized by Hummer's method using natural flake graphite [41, 42]. The concentration of the GO suspension obtained was $2.3 \text{ g}\cdot\text{L}^{-1}$, which was determined by drying the GO suspension at 95°C for 24 h then weighing.

4.2 Graphene-sulfur composite synthesis

For the 3DG-S90 sample, 0.1 mL of 1 M $\text{Na}_2\text{S}_2\text{O}_3$ was first mixed with 0.22 mL of $2.3 \text{ g}\cdot\text{L}^{-1}$ GO suspension and 0.58 mL of deionized water. 0.1 mL of 2 M HCl was added drop-wise to the above solution with stirring for 2 h. 20 μL of 1 M ascorbic acid was added to the prior solution, and heated for 2 h at 95°C to form the hydrogel. After the formation of the 3DG-S composite hydrogel, it was washed several times with water and then freeze-dried. The amounts of the $\text{Na}_2\text{S}_2\text{O}_3$ and HCl were tuned to synthesize 3DG-S70, 80 and 95 using the same method.

4.3 Materials characterization

Scanning electron microscopy (SEM JEOL 6700) was used to study the morphology of the sulfur cathode. Transmission electron microscopy (TEM T12 Quick CryoEM) was taken to investigate the sulfur infused within the 3D graphene pockets. XRD was carried out using a Panalytical X'Pert Pro X-ray Powder Diffractometer with Cu Ka radiation. X-ray photoelectron spectroscopy (Axis Ultra DLD) was used to probe the interactions between sulfur and graphene. TGA was carried out to evaluate the sulfur loading amount using PerkinElmer instruments Pyris Diamond TG/DTA.

4.4 Electrochemical testing

The electrochemical properties were carried out by assembly of CR2025 coin cells in an argon filled glovebox with water and oxygen content kept below 0.1 ppm. The mechanically pressed 3DG-S samples with thickness around $100 \mu\text{m}$ were directly used as the cathodes and lithium foil was used as the anodes. The electrolyte was a solution of lithium bis(trifluoromethanesulfonyl)imide (1 M) in 1:1 (*v/v*) 1,2-dimethoxyethane (DME) and 1,3-dioxolane (DOL) containing LiNO_3 (1 wt.%). For a typical 3DG-90 cathode, the area was 0.636 cm^2 (the disk with a diameter of 9 mm) and the sulfur mass loading of 3DG-S90 was $4.32 \text{ mg}\cdot\text{cm}^{-2}$. Galvanostatic charge/discharge cycling was carried out in a potential range of 1.6–2.6 V vs. Li/Li⁺ with a multichannel battery testing system (LAND CT2001A).

Acknowledgements

We acknowledge the Electron Imaging Center for Nanomachines (EICN) at the California NanoSystems Institute for the technical support of TEM. X. F. D. acknowledges partial support by a Dupont Young Professor Award. X. X. would like to acknowledge the Chinese Scholarship Council (CSC) for financial support.

Electronic Supplementary Material: Supplementary material (TGA of rGO, video of sulfur melting within

graphene pocket, and comparison table) is available in the online version of this article at <http://dx.doi.org/10.1007/s12274-016-1005-1>.

References

- [1] Mizushima, K.; Jones, P. C.; Wiseman, P. J.; Goodenough, J. B. Li_xCoO_2 ($0 < x \leq 1$): A new cathode material for batteries of high energy density. *Mater. Res. Bull.* **1980**, *15*, 783–789.
- [2] Yamada, A.; Chung, S.-C.; Hinokuma, K. Optimized LiFePO_4 for lithium battery cathodes. *J. Electrochem. Soc.* **2001**, *148*, A224–A229.
- [3] Armand, M.; Tarascon, J.-M. Building better batteries. *Nature* **2008**, *451*, 652–657.
- [4] Tarascon, J.-M.; Armand, M. Issues and challenges facing rechargeable lithium batteries. *Nature* **2001**, *414*, 359–367.
- [5] Bruce, P. G.; Freunberger, S. A.; Hardwick, L. J.; Tarascon, J.-M. Li-O_2 and Li-S batteries with high energy storage. *Nat. Mater.* **2012**, *11*, 19–29.
- [6] Yang, Y.; Zheng, G. Y.; Cui, Y. Nanostructured sulfur cathodes. *Chem. Soc. Rev.* **2013**, *42*, 3018–3032.
- [7] Ji, X. L.; Lee, K. T.; Nazar, L. F. A highly ordered nanostructured carbon–sulphur cathode for lithium–sulphur batteries. *Nat. Mater.* **2009**, *8*, 500–506.
- [8] He, G.; Ji, X. L.; Nazar, L. High “C” rate Li-S cathodes: Sulfur imbibed bimodal porous carbons. *Energy Environ. Sci.* **2011**, *4*, 2878–2883.
- [9] Lin, T. Q.; Tang, Y. F.; Wang, Y. M.; Bi, H.; Liu, Z. Q.; Huang, F. Q.; Xie, X. M.; Jiang, M. H. Scotch-tape-like exfoliation of graphite assisted with elemental sulfur and graphene–sulfur composites for high-performance lithium–sulfur batteries. *Energy Environ. Sci.* **2013**, *6*, 1283–1290.
- [10] Manthiram, A.; Fu, Y. Z.; Chung, S.-H.; Zu, C. X.; Su, Y.-S. Rechargeable lithium–sulfur batteries. *Chem. Rev.* **2014**, *114*, 11751–11787.
- [11] Zhang, S. S. Liquid electrolyte lithium/sulfur battery: Fundamental chemistry, problems, and solutions. *J. Power Sources* **2013**, *231*, 153–162.
- [12] Ji, X. L.; Nazar, L. F. Advances in Li-S batteries. *J. Mater. Chem.* **2010**, *20*, 9821–9826.
- [13] Zang, J.; An, T. H.; Dong, Y. J.; Fang, X. L.; Zheng, M. S.; Dong, Q. F.; Zheng, N. F. Hollow-in-hollow carbon spheres with hollow foam-like cores for lithium–sulfur batteries. *Nano Res.* **2015**, *8*, 2663–2675.
- [14] Zhang, K.; Zhao, Q.; Tao, Z. L.; Chen, J. Composite of sulfur impregnated in porous hollow carbon spheres as the cathode of Li-S batteries with high performance. *Nano Res.* **2013**, *6*, 38–46.
- [15] Qiu, Y. C.; Li, W. F.; Li, G. Z.; Hou, Y.; Zhou, L. S.; Li, H. F.; Liu, M. N.; Ye, F. M.; Yang, X. W.; Zhang, Y. G. Polyaniline-modified cetyltrimethylammonium bromide–graphene oxide–sulfur nanocomposites with enhanced performance for lithium–sulfur batteries. *Nano Res.* **2014**, *7*, 1355–1363.
- [16] Li, Z.; Jiang, Y.; Yuan, L. X.; Yi, Z. Q.; Wu, C.; Liu, Y.; Strasser, P.; Huang, Y. H. A highly ordered meso@microporous carbon-supported sulfur@smaller sulfur core–shell structured cathode for Li-S batteries. *ACS Nano* **2014**, *8*, 9295–9303.
- [17] Lv, D. P.; Zheng, J. M.; Li, Q. Y.; Xie, X.; Ferrara, S.; Nie, Z. M.; Mehdi, L. B.; Browning, N. D.; Zhang, J. G.; Graff, G. L. et al. High energy density lithium–sulfur batteries: Challenges of thick sulfur cathodes. *Adv. Energy Mater.* **2015**, *5*, 1402290.
- [18] Cheng, X.-B.; Huang, J.-Q.; Zhang, Q.; Peng, H.-J.; Zhao, M.-Q.; Wei, F. Aligned carbon nanotube/sulfur composite cathodes with high sulfur content for lithium–sulfur batteries. *Nano Energy* **2014**, *4*, 65–72.
- [19] Lu, S. T.; Chen, Y.; Wu, X. H.; Wang, Z. D.; Li, Y. Three-dimensional sulfur/graphene multifunctional hybrid sponges for lithium–sulfur batteries with large areal mass loading. *Sci. Rep.* **2014**, *4*, 4629.
- [20] Evers, S.; Nazar, L. F. Graphene-enveloped sulfur in a one pot reaction: A cathode with good coulombic efficiency and high practical sulfur content. *Chem. Commun.* **2012**, *48*, 1233–1235.
- [21] Zheng, J. M.; Gu, M.; Wagner, M. J.; Hays, K. A.; Li, X. H.; Zuo, P. J.; Wang, C. M.; Zhang, J.-G.; Liu, J.; Xiao, J. Revisit carbon/sulfur composite for Li-S batteries. *J. Electrochem. Soc.* **2013**, *160*, A1624–A1628.
- [22] Xu, G.-L.; Xu, Y.-F.; Fang, J.-C.; Peng, X.-X.; Fu, F.; Huang, L.; Li, J.-T.; Sun, S.-G. Porous graphitic carbon loading ultra high sulfur as high-performance cathode of rechargeable lithium–sulfur batteries. *ACS Appl. Mat. Interfaces* **2013**, *5*, 10782–10793.
- [23] Nazar, L. F.; Cuisinier, M.; Pang, Q. Lithium–sulfur batteries. *MRS Bull.* **2014**, *39*, 436–442.
- [24] Xu, Y. X.; Sheng, K. X.; Li, C.; Shi, G. Q. Self-assembled graphene hydrogel via a one-step hydrothermal process. *ACS Nano* **2010**, *4*, 4324–4330.
- [25] Tang, Z. H.; Shen, S. L.; Zhuang, J.; Wang, X. Noble-metal-promoted three-dimensional macroassembly of single-layered graphene oxide. *Angew. Chem., Int. Ed.* **2010**, *49*, 4603–4607.
- [26] Xu, Y. X.; Shi, G. Q.; Duan, X. F. Self-assembled three-dimensional graphene macrostructures: Synthesis and applications in supercapacitors. *Acc. Chem. Res.* **2015**, *48*, 1666–1675.

- [27] Xu, Y. X.; Chen, C.-Y.; Zhao, Z. P.; Lin, Z. Y.; Lee, C.; Xu, X.; Wang, C.; Huang, Y.; Shakir, M. I.; Duan, X. F. Solution processable holey graphene oxide and its derived macrostructures for high-performance supercapacitors. *Nano Lett.* **2015**, *15*, 4605–4610.
- [28] Xu, Y. X.; Lin, Z. Y.; Huang, X. Q.; Liu, Y.; Huang, Y.; Duan, X. F. Flexible solid-state supercapacitors based on three-dimensional graphene hydrogel films. *ACS Nano* **2013**, *7*, 4042–4049.
- [29] Xu, Y. X.; Lin, Z. Y.; Huang, X. Q.; Wang, Y.; Huang, Y.; Duan, X. F. Functionalized graphene hydrogel-based high-performance supercapacitors. *Adv. Mater.* **2013**, *25*, 5779–5784.
- [30] Xu, Y. X.; Huang, X. Q.; Lin, Z. Y.; Zhong, X.; Huang, Y.; Duan, X. F. One-step strategy to graphene/Ni(OH)₂ composite hydrogels as advanced three-dimensional supercapacitor electrode materials. *Nano Res.* **2013**, *6*, 65–76.
- [31] Xu, Y. X.; Lin, Z. Y.; Zhong, X.; Huang, X. Q.; Weiss, N. O.; Huang, Y.; Duan, X. F. Holey graphene frameworks for highly efficient capacitive energy storage. *Nat. Commun.* **2014**, *5*, 4554.
- [32] Kim, H.; Lim, H.-D.; Kim, J.; Kang, K. Graphene for advanced Li/S and Li/air batteries. *J. Mater. Chem. A* **2014**, *2*, 33–47.
- [33] Zhou, G. M.; Yin, L.-C.; Wang, D.-W.; Li, L.; Pei, S. F.; Gentle, I. R.; Li, F.; Cheng, H.-M. Fibrous hybrid of graphene and sulfur nanocrystals for high-performance lithium–sulfur batteries. *ACS Nano* **2013**, *7*, 5367–5375.
- [34] Xi, K.; Kidambi, P. R.; Chen, R. J.; Gao, C. L.; Peng, X. Y.; Ducati, C.; Hofmann, S.; Kumar, R. V. Binder free three-dimensional sulphur/few-layer graphene foam cathode with enhanced high-rate capability for rechargeable lithium sulphur batteries. *Nanoscale* **2014**, *6*, 5746–5753.
- [35] Gao, X. F.; Li, J. Y.; Guan, D. S.; Yuan, C. A scalable graphene sulfur composite synthesis for rechargeable lithium batteries with good capacity and excellent columbic efficiency. *ACS Appl. Mat. Interfaces* **2014**, *6*, 4154–4159.
- [36] Sun, L.; Li, M. Y.; Jiang, Y.; Kong, W. B.; Jiang, K. L.; Wang, J. P.; Fan, S. S. Sulfur nanocrystals confined in carbon nanotube network as a binder-free electrode for high-performance lithium sulfur batteries. *Nano Lett.* **2014**, *14*, 4044–4049.
- [37] Chen, H. W.; Wang, C. H.; Dong, W. L.; Lu, W.; Du, Z. L.; Chen, L. W. Monodispersed sulfur nanoparticles for lithium–sulfur batteries with theoretical performance. *Nano Lett.* **2015**, *15*, 798–802.
- [38] Xu, R.; Lu, J.; Amine, K. Progress in mechanistic understanding and characterization techniques of Li–S batteries. *Adv. Energy Mater.* **2015**, *5*, 1500408.
- [39] Manthiram, A.; Chung, S. H.; Zu, C. X. Lithium–sulfur batteries: Progress and prospects. *Adv. Mater.* **2015**, *27*, 1980–2006.
- [40] Li, W. Y.; Liang, Z.; Lu, Z. D.; Yao, H. B.; Seh, Z. W.; Yan, K.; Zheng, G. Y.; Cui, Y. A sulfur cathode with pomegranate-like cluster structure. *Adv. Energy Mater.* **2015**, *5*, 1500211.
- [41] Hummers Jr, W. S.; Offeman, R. E. Preparation of graphitic oxide. *J. Am. Chem. Soc.* **1958**, *80*, 1339–1339.
- [42] Xu, Y. X.; Zhao, L.; Bai, H.; Hong, W. J.; Li, C.; Shi, G. Q. Chemically converted graphene induced molecular flattening of 5,10,15,20-tetrakis(1-methyl-4-pyridinio)porphyrin and its application for optical detection of cadmium(II) ions. *J. Am. Chem. Soc.* **2009**, *131*, 13490–13497.